Available online at ScienceDirect

ScienceDirect

J. Mater. Sci. Technol., 2014, 30(8), 743–747

JMST

www.JMST.org

Dielectric and Ferroelectric Properties of $BaTiO_3$ Nanofibers Prepared via Electrospinning

Yan Wei[1)*], *Yu Song*[2)], *Xuliang Deng*[1)], *Bing Han*[1)], *Xuehui Zhang*[2)], *Yang Shen*[2)**], *Yuanhua Lin*[2)]

1) Department of Geriatric Dentistry, School and Hospital of Stomatology, Peking University, Beijing 100081, China

2) School of Materials Science and Engineering, and State Key Lab of New Ceramics and Fine Processing, Tsinghua University, Beijing 100084, China

[Manuscript received August 15, 2013, in revised form October 13, 2013, Available online 5 April 2014]

$BaTiO_3$ nanofibers of about 400 nm in diameter were synthesized via electrospinning. The evolution of the morphology and phase composition of the $BaTiO_3$ nanofibers was studied by scanning electron microscopy and X-ray diffraction within the annealing temperature of 750–1050 °C. Higher annealing temperature led to rougher surface and better crystallization of the $BaTiO_3$ nanofibers. Below 1050 °C, the $BaTiO_3$ nanofibers maintained its large aspect ratios and could still be regarded as individual nanofiber. The dielectric permittivities of the $BaTiO_3$ nanofibers ($\varepsilon_r \sim 820$) were calculated with the MG equation by considering the porous bulk specimens as composites of $BaTiO_3$ nanofibers and air. The ferroelectric properties of the $BaTiO_3$ nanofibers were measured by using a ferroelectric analyzer coupled with an atomic force microscope. *P–E* loop measured for the $BaTiO_3$ nanofiber exhibits small hysteresis.

KEY WORDS: Dielectric; Ferroelectric; Barium titanate; Electrospinning

1. Introduction

$BaTiO_3$ is studied as a typical ferroelectric material with high dielectric permittivity, low dielectric loss and other excellent ferroelectric properties[1]. Owing to the outstanding properties, $BaTiO_3$ has been widely applied in capacitors, sensors, nonvolatile random access memory and many composites[2]. With their high intrinsic dielectric permittivities, the nanostructured $BaTiO_3$ particles, such as spheres[3] or fibers[4], have also been employed as dielectric fillers in polymer composites to improve the dielectric behavior of the composites. The dielectric as well as geometric (size, shape etc) properties of the $BaTiO_3$ particles play a critical role in determining the dielectric behavior of the polymer composites[5,6]. There have also been efforts in making three-phase polymer composites filled with both $BaTiO_3$ particles and conductive fillers. The presence of $BaTiO_3$ nanoparticles prevents the conductive fillers from connecting into conducting paths, giving rise to lower dielectric loss. Our recent results show that a kind of three-phase polymer composite filled with $BaTiO_3$ nanoparticles and graphene nanopellets could be polarized up to 150 kV/mm without much increased leakage current[7]. Yet, $BaTiO_3$ nanofibers are considered more promising over their spherical counterparts as dielectric fillers to improve the dielectric strength of their composites with polymers under high electric field. Due to their large aspect ratios and hence larger dipolar moment along their longitudinal axis, $BaTiO_3$ nanofibers are capable of increasing the dielectric permittivity of polymer composites[8]. Recent studies further indicate that surface treatments of $BaTiO_3$ nanofibers leads to stronger interfaces between the nanofibers and polymer matrix, giving rise to enhanced dielectric breakdown strength of polymer composites[9]. Enhanced dielectric strength of these $BaTiO_3$ nanofibers-filled polymer composites is attributed to the orientation of $BaTiO_3$ nanofibers in directions perpendicular to the external electric field. Both phase field modeling[6] and finite element simulation[10] indicate that the orientation of $BaTiO_3$ nanofibers is favorable for mitigating the electric field concentration in polymer matrix, which is caused by the large differences in dielectric permittivity between the $BaTiO_3$ ($\varepsilon_r \sim 1000$) and polymer matrix ($\varepsilon_r \sim 2–3$).

Electrospinning is one of the methods to fabricate one-dimensional materials. It is a convenient and versatile method to produce fibers, for instance, polymer, ceramic and composite fibers[11–14]. In this study, continuous $BaTiO_3$ nanofibers are prepared via electrospinning with sol–gel precursor.

* Corresponding author. Ph.D.; E-mail address: kqdxl@bjmu.edu.cn (Y. Wei).

** Corresponding author. Prof., Ph.D.; Tel.: +86 10 62773300; E-mail address: shyang_mse@tsinghua.edu.cn (Y. Shen).

http://dx.doi.org/10.1016/j.jmst.2014.03.021

Dielectric and ferroelectric properties of $BaTiO_3$ ceramics have been intensively studied and well documented. The measurements are usually performed to dense ceramics sintered at relatively high temperature. There have been very limited reports on the dielectric behavior of $BaTiO_3$ nanofibers[15]. Although piezoelectric force microscopy (PFM) has been employed for the measurement of the piezoelectric response of the aligned $BaTiO_3$ nanofibers[16], the measurement of their dielectric permittivities still requires a bulk specimen which is normally obtained through sintering at high temperature. The dielectric behavior obtained from a dense body thus could not be regarded as the intrinsic dielectric permittivities of the individual $BaTiO_3$ nanofibers. Here, in this contribution, we explored the evolution of morphology and phase composition of $BaTiO_3$ nanofibers with annealing temperature up to 1050 °C, the upper limit beyond which the $BaTiO_3$ nanofibers are sintered into bundles or cluster and can't be treated as individual nanofibers. Porous bulk specimens of the $BaTiO_3$ nanofibers are calcined at <1050 °C with their dielectric permittivities measured. The dielectric permittivities of the individual $BaTiO_3$ nanofibers are then calculated with a Maxwell–Garnett equation by considering the specimens as composites of $BaTiO_3$ nanofibers and air. The ferroelectric properties of the $BaTiO_3$ nanofibers are also investigated by using a ferroelectric test module coupled with an atomic force microscope (AFM).

2. Experimental

The chemicals were purchased from China National Medicines Corporation Ltd. if not otherwise specified. $BaTiO_3$ nanofibers were prepared via electrospinning combined with sol–gel method. Briefly, barium acetate, tetrabutyl titanate and acetylacetone were dissolved in acetic acid at a molar ratio of 1:1:2 and stirred to get homogeneous barium titanate precursor sol. Poly (vinyl pyrrolidone) (PVP, $M = 1{,}300{,}000$) was added to the precursor for the control of sol viscosity. The sol was then transferred into a syringe and electrospun by applying an electric field of 1.5 kV/cm. Fibers consisting of PVP and barium titanate precursor via electrospinning were then calcined at 550 °C for 1.5 h to remove PVP. White powders were obtained. For direct comparison, $BaTiO_3$ particles were also prepared with the sol of barium titanate precursor and PVP by calcining at 550 °C for 1.5 h. Both the $BaTiO_3$ nanofibers and $BaTiO_3$ particles were annealed at 750 °C, 850 °C, 950 °C and 1050 °C for 6 h.

For the measurement of dielectric properties, the $BaTiO_3$ nanofibers were cold-pressed into pellets of 10 mm in diameter at 2 MPa. The resultant pellets were thermally treated at 750 °C, 850 °C, 950 °C and 1050 °C for 6 h, respectively. Ag paste was then painted on both sides of the pellet samples as electrodes for the measurement of dielectric properties. The apparent densities (ρ_a) of the resultant sample pellets after each heat treatment were measured by Archimedes method. The theoretical densities (ρ_t) of $BaTiO_3$ specimens were also determined from the XRD patterns. The relative density was then determined as ρ_a/ρ_t.

X-Ray diffraction (XRD, Bruker D8) and scanning electron microscopy (SEM, JEOL4500) were employed to investigate the crystal structure and morphology of $BaTiO_3$ fibers and particles. Dielectric properties were measured by employing an HP 4294A precision impedance analyzer (Agilent) in the frequency range of 100 Hz to 100 MHz at room temperature. For the measurement of the ferroelectric properties, the $BaTiO_3$ nanofibers were glued to a Pt/Si substrate with silver paste as bottom electrode and grounded. The probe of the atomic force microscope (AFM, PISA XE-100) was connected to a ferroelectric test module (TF analyzer 2000, axiACCT) and used as top electrode. During the measurement, topography image of the $BaTiO_3$ nanofibers was firstly obtained by AFM image and was then used to navigate the probe to touch the top of the $BaTiO_3$ nanofiber. The polarization–electric field (P–E) loops were then measured by the ferroelectric test module at 20 Hz.

3. Results and Discussion

The effects of annealing temperature on the evolution of morphology of $BaTiO_3$ nanofibers are first characterized by SEM. Fig. 1(a)–(d) shows the SEM images of $BaTiO_3$ nanofibers calcined at different temperatures. As the temperature increases from 750 °C to 1050 °C, the diameter of the $BaTiO_3$ nanofibers gradually decreases from ~800 nm to ~400 nm, which is also accompanied by the change of surface morphology of the nanofibers from quite smooth at 750 °C to rather rough at 1050 °C. The morphology evolution of $BaTiO_3$ nanofibers with temperature are in line with the trend observed by others. Li et al. reported the same change in surface roughness of the $BaTiO_3$ nanofibers after annealing from 500 °C to 800 °C[17]. Within this temperature range, the $BaTiO_3$ nanofibers undergo the transformation from amorphous to crystalline. With the further increase of annealing temperature up to 1050 °C, the $BaTiO_3$ nanofibers begin to sinter, giving rise to even rougher surface and much less pores in the nanofibers. For comparison, the $BaTiO_3$ particles derived from the same precursor sol used in the electrospinning process are subjected to the same heat treatments with their SEM images shown in Fig. 1(e)–(h). The most distinctive change in morphology of the $BaTiO_3$ particles could be observed in the sample annealed at 1050 °C (Fig. 1(h)), where most of the particles have been sintered into large clusters.

In addition to the evolution of the morphology of $BaTiO_3$ nanofibers with annealing temperature, phase transformation from cubic to tetragonal is also revealed by X-Ray diffraction patterns, as shown in Fig. 2. On the XRD patterns of samples annealed at 750 °C and 850 °C, all diffraction peaks could be assigned to cubic phase (space group: Pm3m). Further increase in the annealing temperature to 950 °C and 1050 °C leads to the phase transformation from cubic to tetragonal (space group: P4mm), as evidenced by the split of (200) and (311) peaks of cubic phase (as better distinguished in Fig. 2(b) and (c)). The same phase transformation is observed in the $BaTiO_3$ particles after the same heat treatments, with the only difference being the higher tetragonality of the $BaTiO_3$ nanofibers than that of the $BaTiO_3$ particles. As calculated from the XRD patterns, c/a ratio of $BaTiO_3$ fibers are 1.0083 at 950 °C and 1.0084 at 1050 °C, as compared with c/a of ~1.0076 at 950 °C and 1.0081 at 1050 °C for $BaTiO_3$ particles. Also It could be observed from the XRD patterns that the intensities of the (002)/(200) peaks and (113)/(311) peaks are much higher in the $BaTiO_3$ nanofibers than those in the $BaTiO_3$ particles (as shown in Fig. 2(b)–(f)), which is indicative of better crystallization after the annealing. The better crystallization of $BaTiO_3$ nanofibers is further evidenced by their larger grain sizes as compared with the $BaTiO_3$ particles. Fig. 3 shows the variation of grain size determined from the XRD patterns with annealing temperature. As seen in both the $BaTiO_3$ nanofibers and $BaTiO_3$ particles, the grain size consistently increases with increasing annealing temperature. The grain size of the $BaTiO_3$ nanofibers is larger than that of the $BaTiO_3$ particles at all temperatures.

Dielectric behaviors of both the $BaTiO_3$ nanofibers and particles are measured from the porous bulk specimen. With the

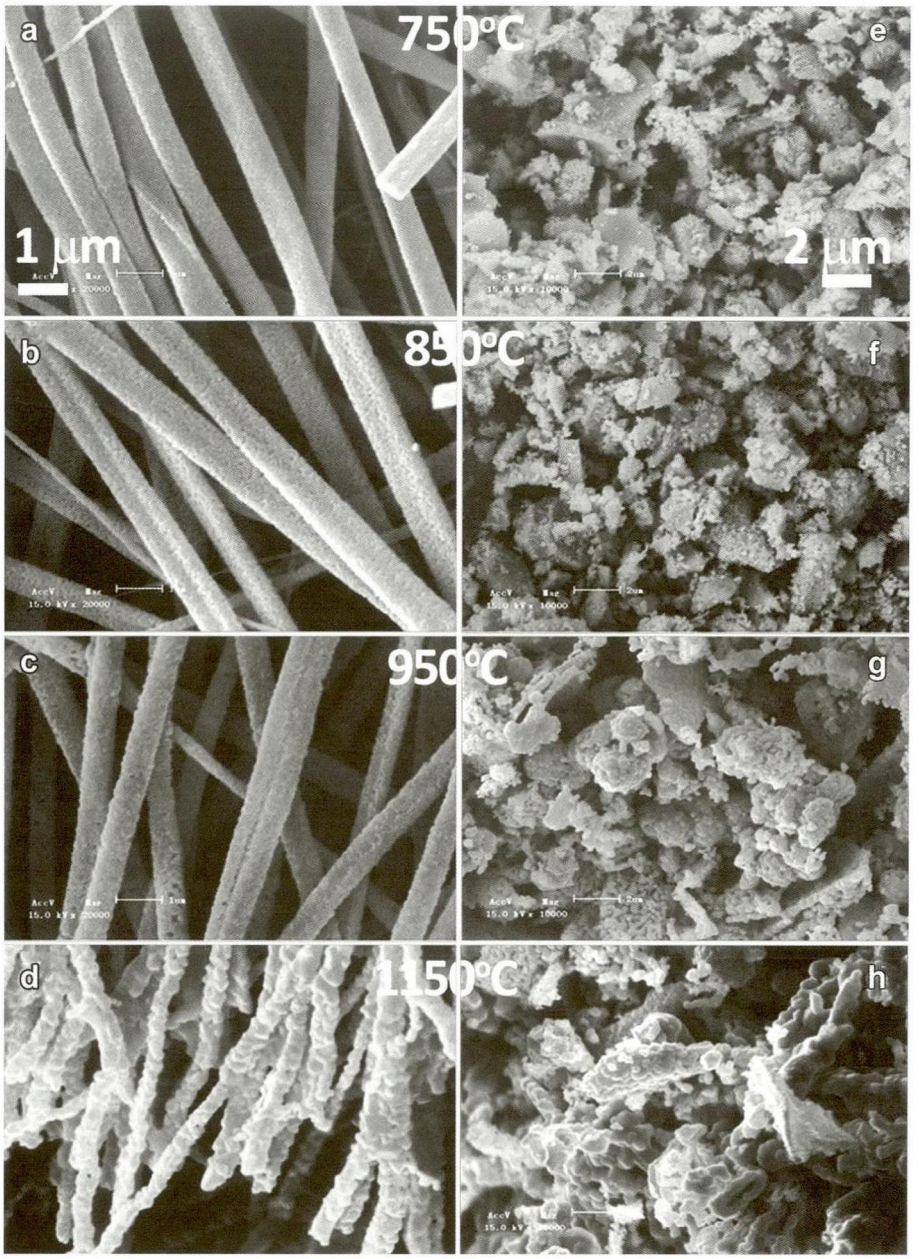

Fig. 1 SEM images of the $BaTiO_3$ nanofibers/particles calcined at 750 °C (a and e), 850 °C (b and f), 950 °C (c and g) and 1050 °C (d and h) for 6 h.

presence of pores in the specimen, the dielectric permittivities of these specimens are rather low, i.e., only ~200 even for the specimen that has been annealed at 1050 °C. Two features can be readily observed from the frequency dependence of dielectric permittivities shown in Fig. 4(a). First, the dielectric permittivies remain stable within the frequency range of 100−10 MHz, suggesting no dielectric relaxation processes. Second, the dielectric permittivity increases with increasing annealing temperature for both the $BaTiO_3$ nanofibers and particles. In addition, the dielectric permittivities of the $BaTiO_3$ nanofibers are consistently higher than their particle counterparts at all temperatures. For the determination of dielectric permittivities of the $BaTiO_3$ nanofibers, the porous specimens are considered as composites of $BaTiO_3$ nanofibers and air. The dielectric permittivity of the $BaTiO_3$ nanofibers can then be calculated by the Maxwell-Garnett equation as[18]:

$$\frac{\varepsilon_r - \varepsilon_i}{\varepsilon_r + 2\varepsilon_i} = f_a \cdot \frac{\varepsilon_a - \varepsilon_i}{\varepsilon_a + 2\varepsilon_i} \quad (1)$$

where ε_r is the apparent dielectric permittivity of the specimen, ε_i the intrinsic dielectric permittivity of the $BaTiO_3$ nanofibers, ε_a the air dielectric permittivity of ~1. $f_a = 1 - \rho_a/\rho_t$ is the volume fraction of air. The intrinsic dielectric permittivities calculated by the MG equation are plotted as a function of annealing temperatures in Fig. 4(b). In general, higher annealing temperature results in higher dielectric permittivities, both for the $BaTiO_3$ nanofibers and particles. Highest dielectric permittivity of

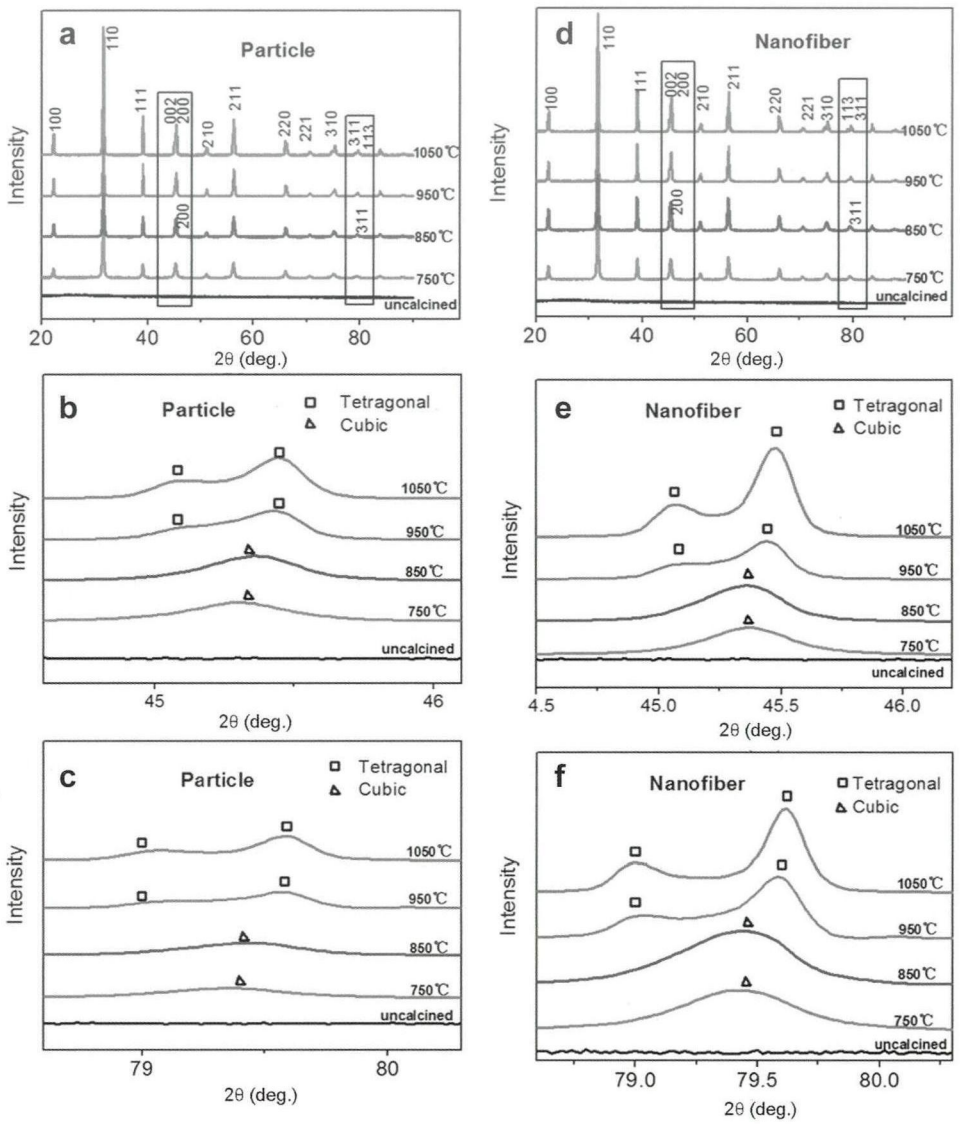

Fig. 2 X-Ray diffraction patterns for the $BaTiO_3$ nanofibers (a) and the $BaTiO_3$ particles (b) after annealing at different temperatures. The phase transformation from cubic to tetragonal is better distinguished by the splitting of (200) peak into (200)/(002) peaks (c & d) and (311) peak into (311)/(113) peaks (e & f).

~820 is obtained for the $BaTiO_3$ nanofibers annealed at 1050 °C, which is comparable with the dielectric permittivities of the dense $BaTiO_3$ ceramic with an average grain size of ~ 20 nm[19]. Given the larger grain size of the $BaTiO_3$ nanofibers, the dielectric permittivity of the $BaTiO_3$ nanofibers, is still much smaller than the dielectric permittivity of the well sintered $BaTiO_3$ ceramics (usually >1000)[20]. Two factors have to be considered when discussing these results. The first one is that the $BaTiO_3$ nanofibers are treated at temperatures much lower than the sintering temperature. The interface between the $BaTiO_3$ nanofibers and air could have adverse effects on the dielectric behavior of the specimen. Moreover, given the rather high volume fraction of air in the porous specimen, the MG equation could underestimate the real dielectric permittivities of the $BaTiO_3$ nanofibers[18]. The dielectric permittivities thus determined should be considered as the lower limit for the intrinsic dielectric permittivities of the $BaTiO_3$ nanofibers.

Fig. 5 shows the polarization−electric field (P−E) loop for the $BaTiO_3$ nanofiber. The P−E loop exhibits very small hysteresis with almost linear dependence of $P(E)$, more of the paraelectric behavior than ferroelectric. The strong suppression of macroscopic ferroelectric character for the $BaTiO_3$ nanofibers could be attributed to the following causes. First, the frozen domain structure under an external field owing to the effects exerted by the grain boundaries,

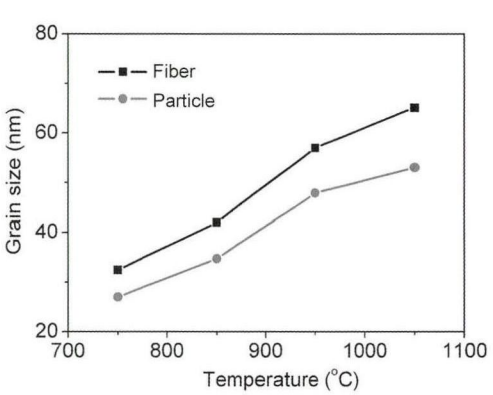

Fig. 3 Variation of the grain sizes of $BaTiO_3$ nanofibers and particles with annealing temperatures.

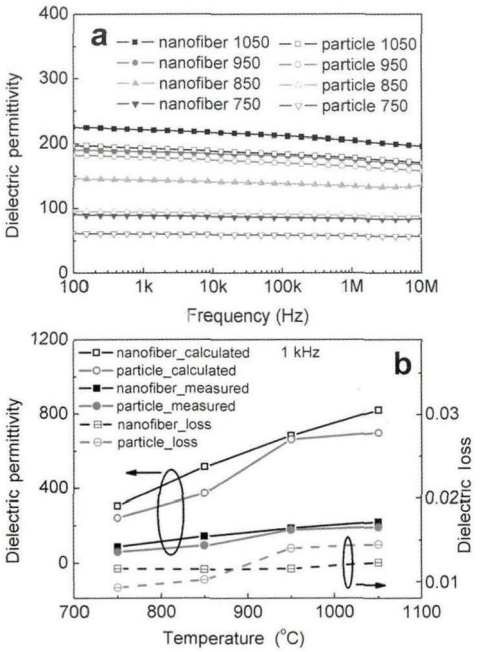

Fig. 4 (a) Dependences of dielectric permittivity on frequency from 100 Hz to 10 MHz of $BaTiO_3$ nanofibers and particles after annealing at different temperatures. (b) Dielectric permittivities calculated by the MG equation for $BaTiO_3$ nanofibers and particles after annealing at different temperatures at 1 kHz. The variation of dielectric loss with annealing temperatures is also superimposed.

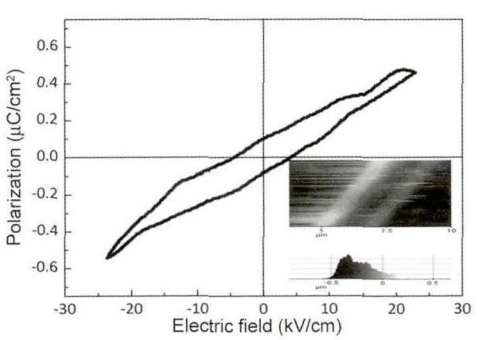

Fig. 5 Polarization−electric field loop for the $BaTiO_3$ nanofiber annealed at 1050 °C. The inset shows the topography image of the $BaTiO_3$ nanofiber measured.

such as the clamping of the domain walls and the hindrance of polarization switching, plays a key role in the suppression of ferroelectric hysteresis and switching[21]. Next, the depolarization field originated by the low permittivity nonferroelectric grain boundaries can cause a significant reduction of polarization[22]. It is also worth noting that the *P*−*E* loop obtained in this manner only represents the polarization behavior in the direction of the short axle of the $BaTiO_3$ nanofibers. With the large differences in the depolarization field along the longitudinal direction and the lateral directions of the $BaTiO_3$ nanofibers, as calculated by Wang et al.[6], the polarization behaviors of the $BaTiO_3$ nanofibers along the longitudinal direction might be much different.

4. Conclusion

In summary, $BaTiO_3$ nanofibers of diameters around 400 nm are synthesized via electrospinning, and their dielectric and ferroelectric properties are investigated. Below 1050 °C, $BaTiO_3$ nanofibers maintain its large aspect ratio and still can be regarded as individual fiber. $BaTiO_3$ nanofibers are better crystallized as compared with the $BaTiO_3$ particles after the same heat treatments. The dielectric permittivities of the $BaTiO_3$ nanofibers are calculated with the MG equation by considering the porous bulk specimens as composites of $BaTiO_3$ nanofibers and air. The *P*−*E* loop measured for the $BaTiO_3$ nanofiber exhibits small hysteresis. Further investigation is still needed for the determination of the polarization behavior of the $BaTiO_3$ nanofibers along their longitudinal direction.

Acknowledgments

The authors acknowledge financial supports from the National Basic Research Program of China (No. 2012CB933900), the Key Technologies R&D Program of China (No. 2012BAI07B00), the National High Technology Research and Development Program of China (No. 2011AA030100) and the Foundation for the Authors of National Excellent Doctoral Dissertations of China (Grant No. 201144), Beiing Nova Program (Grant No. XX2013037) and Tsinghua University (Grant No. 20121087925).

REFERENCES

[1] M.H. Frey, D.A. Payne, Phys. Rev. B 54 (1996) 3158−3168.
[2] S. O'Brien, L. Brus, C.B. Murray, J. Am. Chem. Soc. 123 (2001) 12085−12806.
[3] L. Li, A. Takahashi, J. Hao, R. Kikuchi, T. Hayakawa, T. Tsurumi, M. Kakimoto, IEEE Trans. Comp. Packaging Technol. 28 (2005) 754−759.
[4] Y. Song, Y. Shen, H.Y. Liu, Y.H. Lin, M. Li, C.W. Nan, J. Mater. Chem. 22 (2012) 8063−8068.
[5] Y.U. Wang, Appl. Phys. Lett. 96 (2010) 232901.
[6] Y.U. Wang, D.Q. Tan, J. Krahn, J. Appl. Phys. 110 (2011) 044103.
[7] Y. Shen, Y.H. Guan, Y.H. Hu, Y.H. Lin, C.W. Nan, Appl. Phys. Lett. 103 (2013) 072906.
[8] H.A. Avila, L.A. Ramajo, M.S. Goes, M.M. Roberedo, M.S. Castro, R. Parra, ACS Appl. Mater. Interfaces 5 (2013) 505−510.
[9] Y. Song, Y. Shen, H.Y. Liu, Y.H. Lin, M. Li, C.W. Nan, J. Mater. Chem. 22 (2012) 16491−16496.
[10] Z.P. Wang, J.K. Nelson, H. Hillborg, S. Zhao, L.S. Schadler, Comp. Sci. Technol. 76 (2013) 29−36.
[11] D. Li, J.T. McCann, Y.N. Xia, J. Am. Chem. Soc. 89 (2006) 1861−1869.
[12] H. Wu, D.D. Lin, W. Pan, Appl. Phys. Lett. 89 (2006) 133125.
[13] W.E. Teo, S. Ramakrishna, M. Kotaki, X.M. Mo, Nanotechnology 16 (2005) 918−924.
[14] B. Sahoo, P.K. Panda, Ceram. Int. 38 (2013) 5189−5193.
[15] W.S. Yun, J.J. Urban, Q. Gu, Nano Lett. 2 (2002) 447−450.
[16] P. Sà, J. Barbosa, I. Bdikin, B. Almeida, A.G. Rolo, E.M. Gomes, M. Belsley, A.L. Kholkin, D. Isakov, J. Phys. D: Appl. Phys. 46 (2013) 105304.
[17] H.P. Li, H. Wu, D.D. Lin, W. Pan, J. Am. Ceram. Soc. 92 (2009) 2162−2164.
[18] C.W. Nan, Prog. Mater. Sci. 37 (1993) 1−116.
[19] X.Y. Deng, X.H. Wang, H. Wen, L.L. Chen, L. Chen, L.T. Li, Appl. Phys. Lett. 88 (2006) 252905.
[20] Z. Zhao, V. Buscaglia, M. Viviani, M.T. Buscaglia, L. Mitoseriu, A. Testino, M. Nygren, M. Johnsson, P. Nanni, Phys. Rev. B 70 (2004) 024107.
[21] M.H. Frey, Z. Xu, P. Han, D.A. Payne, Ferroelectrics 337 (1998) 206−207.
[22] M.T. Buscaglia, M. Viviani, V. Buscaglia, L. Mitoseriu, A. Testino, P. Nanni, Z. Zhao, M. Nygren, C. Harnagea, D. Piazza, C. Galassi, Phys. Rev. B 73 (2006) 064114.